The 2023 New Zealand Ground-Motion Database

Jesse A. Hutchinson[1], Chuanbin Zhu[2], Brendon A. Bradley[*2], Robin L. Lee[2], Liam M. Wotherspoon[3], Michael Dupuis[2], Claudio Schill[2], Jason Motha[2], Elena F. Manea[4,5], and Anna E. Kaiser[4]

ABSTRACT

This article summarizes the development of the 2023 New Zealand ground-motion database (NZGMDB). A preceding version was formally used as the central ground-motion database in the ground-motion characterization modeling for the 2022 New Zealand (NZ) National Seismic Hazard Model (NSHM) revision. The database contains ground motions for events with a moment magnitude greater than ~ 3.0 from the years 2000 to the end of 2022. Several challenges associated with NZ earthquake source metadata are explained, including determination of earthquake location, magnitude, tectonic classification, and finite-fault geometry, among others. The site table leverages the site database developed as a part of the 2022 NZ NSHM revision, and several definitions of source-to-site distance are computed for the propagation path table. The ground-motion quality classification was initially assessed using a neural network. Subsequent waveform quality verification was conducted and additional quality criteria were enforced to ensure a sufficiently high-quality database. Standard processing techniques were applied to the ground motions before intensity measure (IM) calculation. IMs in the database include peak ground acceleration, 5%-damped pseudoacceleration response spectra, smoothed Fourier amplitude spectra, and other cumulative and duration-related metrics. The NZGMDB is publicly available and routinely updated as new and higher quality data become available.

KEY POINTS

- A database was developed for ground-motion modeling applications of the 2022 National Seismic Hazard Model (NSHM) revision.
- Details of source, site, path, and record metadata and computed intensity measures are provided.
- The database and corresponding flatfiles for common ground-motion components are publicly available.

Supplemental Material

INTRODUCTION

New Zealand (NZ) is a tectonically diverse country with opposing subduction zones beneath the North and South islands that are joined by the nearly 500 km long right-lateral Alpine fault (e.g., Gledhill *et al.*, 2011, and references therein). For nearly two decades, seismic waveform data have been recorded in NZ with the GeoNet project, and hundreds of thousands of events have been recorded, located, and cataloged. These data can be accessed and downloaded via an International Federation of Digital Seismograph Networks (FDSN) web service with popular tools such as the ObsPy module (Beyreuther *et al.*, 2010; Krischer *et al.*, 2015). The NZ earthquake catalog, including temporal, spatial, depth,

and magnitude constraints can be accessed using the GeoNet Quake Search tool (see Data and Resources).

There have been several large and devastating ruptures since 2009. These include the 2009 moment magnitude M_w 7.8 Dusky Sound, 2010 M_w 7.1 Darfield, 2011 M_w 6.2 Christchurch, and 2016 M_w 7.8 Kaikōura events (Fry *et al.*, 2010; Gledhill *et al.*, 2011; Kaiser *et al.*, 2012, Kaiser, Balfour *et al.*, 2017), among others. The wealth of available data provides the opportunity to evaluate the predictive capabilities of ground-motion models (Lee *et al.*, 2022, 2024), develop NZ-specific adjustments to such models, and/or develop entirely new models (Atkinson, 2022; Stafford, 2022). A comprehensive ground-motion database with associated source, path, and site metadata is an essential

1. Ocean Networks Canada, Victoria, Canada, https://orcid.org/0000-0003-1781-0977 (JAH); 2. University of Canterbury, Canterbury, New Zealand, https://orcid.org/0000-0002-4450-314X (BAB); https://orcid.org/0000-0003-1033-5923 (RLL); https://orcid.org/0000-0002-2119-6909 (MD); https://orcid.org/0009-0009-7156-9425 (CS); https://orcid.org/0000-0003-0472-7939 (JM); 3. University of Auckland, Auckland, New Zealand, https://orcid.org/0000-0002-4883-5328 (LMW); 4. GNS Science Te Pu Ao, Lower Hutt, New Zealand, https://orcid.org/0000-0002-0938-8617 (EFM); https://orcid.org/0000-0002-0458-5451 (AEK); 5. National Institute for Earth Physics, Ilfov, Romania

*Corresponding author: brendon.bradley@canterbury.ac.nz

component needed for such endeavors within the broader ground-motion characterization modeling for the 2022 NZ National Seismic Hazard Model (NSHM) revision (Bradley et al., 2022, 2024; Gerstenberger et al., 2022, 2024).

The Next Generation Attenuation (NGA) projects have produced some of the most comprehensive ground-motion databases to date. The Next Generation Attenuation-West1 Project (NGA-West1) project was the first of the NGA series to develop a large high-quality ground-motion database of global active shallow crustal earthquakes (Chiou et al., 2008). Key features of this pioneering database were uniformly processed ground-motion records and comprehensive metadata associated with ground-motion source, path, and site parameters. This was expanded upon subsequently in NGA-West2 (Ancheta et al., 2014) and the recent NGA-Sub (Mazzoni et al., 2022) projects, as well as other analogs globally. Of particular note is the prior NZ-specific ground-motion database in 2017 developed by Van Houtte et al. (2017) and the accompanying site database of Kaiser, Van Houtte, et al. (2017).

Although only six years have passed since the prior NZ-specific effort of Van Houtte et al. (2017), we identified that additional efforts in record processing and metadata determination and collection would allow for an expanded database, which would provide a valuable resource for NZ ground-motion modeling efforts. Further discussion of the database compared with that of Van Houtte et al. (2017) is provided later in the document. However, in summary, we increase the number of events by a factor of ~18 and the number of three-component records by a factor of ~8.

This article describes the implementation of procedures for developing the New Zealand ground-motion database (NZGMDB) version 3.4 (v.3.4). An earlier NZGMDB v.1.0 was published in 2022 (Hutchinson et al., 2022), and we have since provided regular updates to expand and refine the catalog with the input of the NZ seismic hazard modeling community. The aim of the database is to continue to provide a central resource for analysts and modelers to use in developing and testing seismic hazard models for NZ's geologically diverse settings. The NZGMDB v.1.0 was used as part of the 2022 NZ NSHM revision. Because of this earlier release, we have expanded the database to include the years 2021 and 2022, recalculated quality classification scores and intensity measures (IMs), including Fourier amplitude spectra, for ground motions using updated software and waveform data. Additional information was added throughout the database's constituent tables to aid in quality control and filtering for the analyst community. To ensure the highest quality data, we have implemented several quality control measures, which are elaborated upon in the Verification of accelerometer versus seismometer data section.

OVERVIEW OF THE DATABASE

The 2023 NZGMDB v.3.4 is comprised of multiple tables that collectively define ground-motion IMs and underlying metadata associated with the earthquake rupture, wave propagation path, local site conditions (Wotherspoon et al., 2022), and instrument properties. Additional tables are included for calculated station magnitude and phase arrival information that are used in the determination of key parameters provided in the other tables. Specifically, these tables are organized in a relational database, the schema for which is depicted in Figure 1. The constituent data within the relational database include compiled data from numerous references and databases, along with new data computed as part of this project, as described in the subsequent sections. Flatfiles are provided for user convenience, which summarizes key source, path, and site parameters as well as calculated IMs associated with each ground-motion record.

Presently, the NZGMDB contains high-quality ground motions (defined in the Ground-motion classification section) from earthquakes with moment magnitude greater than ~3.0 over the period from 1 January 2000 to 31 December 2022. The NZGMDB comprises 33,052 ground motions from 5422 earthquakes recorded at 362 different seismic instrument locations (Fig. 2). The magnitude versus source-to-site distance and source depth distributions are shown in Figure 3. Crustal and slab events comprise 73% of earthquakes and 79% of records (Fig. 4).
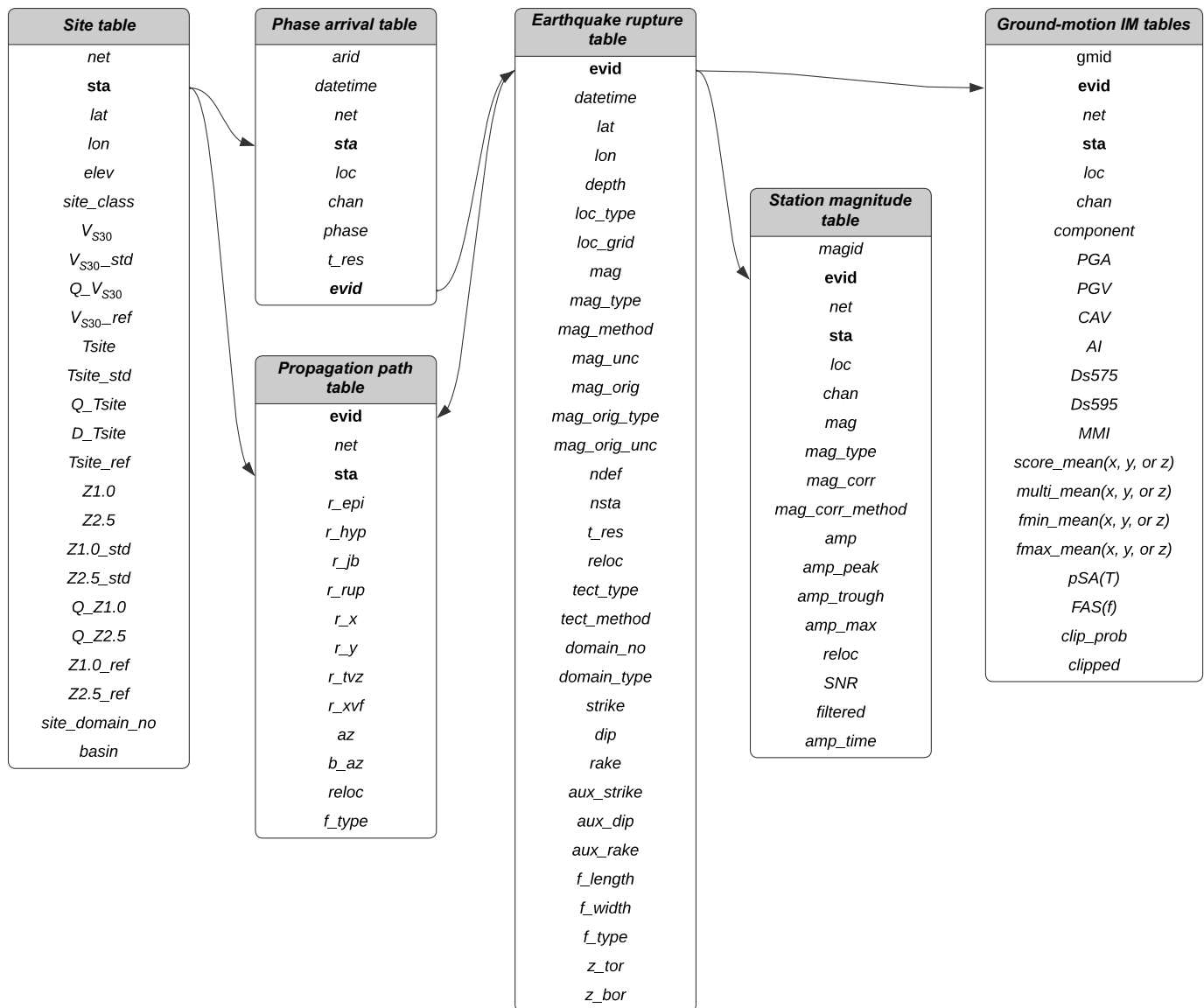
EARTHQUAKE RUPTURE TABLE

The earthquake rupture table includes relevant event parameters for ground-motion modeling, for example, rupture location, magnitude, and other geometric, tectonic, and kinematic variables. Baseline estimates of location and magnitude were collated from the available GeoNet catalog (GeoNet, 2022a). We subsequently harmonized the earthquake rupture table values with respect to location and magnitude, for example, using direct M_w estimates (Ristau, 2013) or, where unavailable, converting local magnitudes (M_L) to a corrected M_L (cM_L) that is equivalent to M_w (Rhoades et al., 2021). A description of earthquake rupture table data fields is provided in Table 1 and is elaborated upon in this section.

Earthquake locations

For many earthquakes (particularly those of small-to-moderate magnitude), earthquake location information is derived from hypocentral locations that are provided as latitude, longitude, and depth coordinates. Unless otherwise indicated by the "reloc" field, the location of these events originates from the GeoNet database (GeoNet, 2022a). The location type ("loc_type") and location grid ("loc_grid") fields of Table 1 provide further information on how hypocenters were determined.

Location type indicates the method used to determine earthquake hypocenters, as provided by the GeoNet database. Before 2012, GeoNet utilized the CUSP location method (Johnson, 1983; Lee and Stewart, 2018) with the GROPE location algorithm. Currently, GeoNet locates earthquakes using the LocSAT (Bratt and Nagy, 1991) and NonLinLoc (Lomax
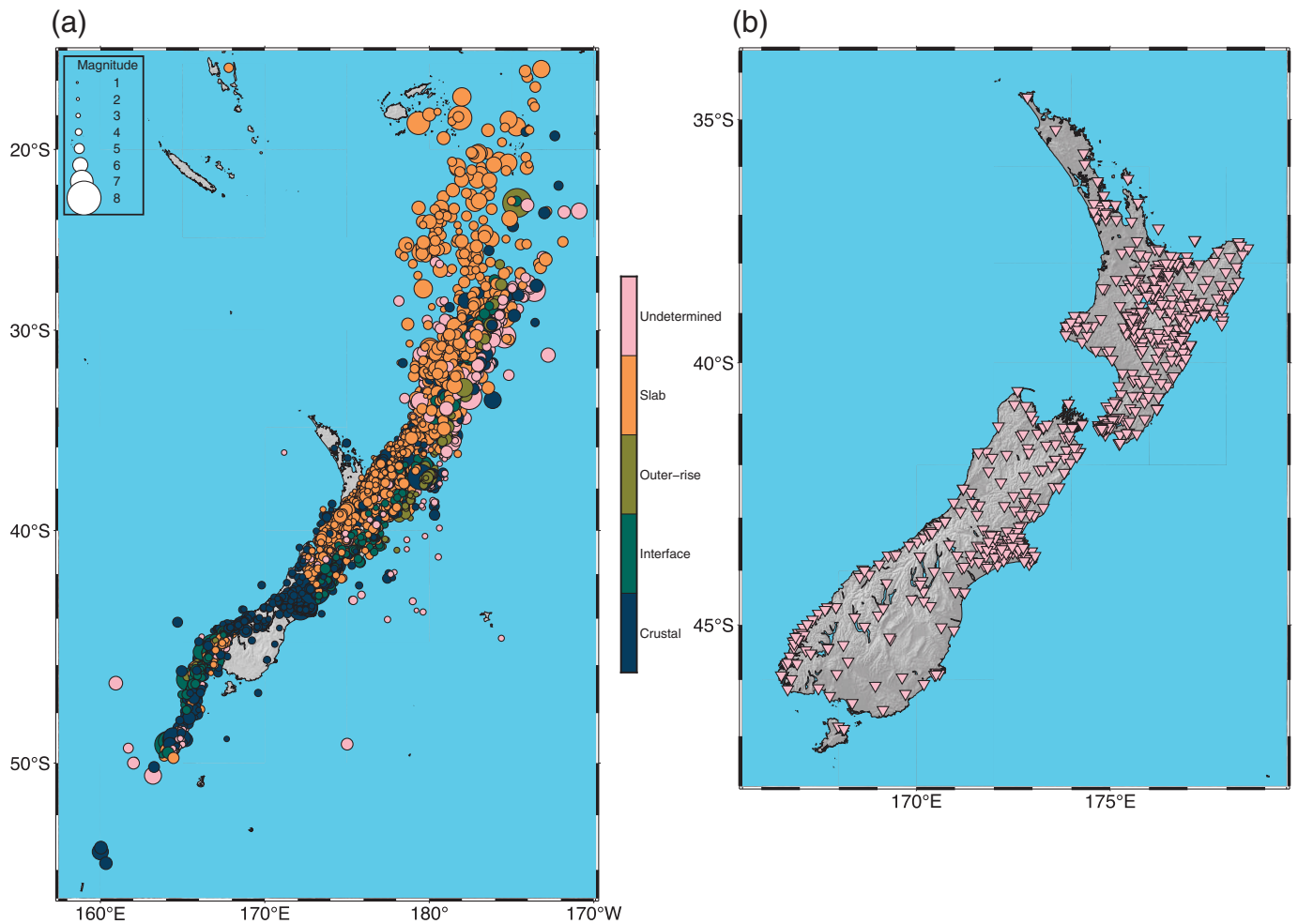
Site table

net
sta
lat
lon
elev
site_class
V_{S30}
V_{S30}_std
Q_V_{S30}
V_{S30}_ref
Tsite
Tsite_std
Q_Tsite
D_Tsite
Tsite_ref
Z1.0
Z2.5
Z1.0_std
Z2.5_std
Q_Z1.0
Q_Z2.5
Z1.0_ref
Z2.5_ref
site_domain_no
basin

Phase arrival table

arid
datetime
net
sta
loc
chan
phase
t_res
evid

Propagation path table

evid
net
sta
r_epi
r_hyp
r_jb
r_rup
r_x
r_y
r_tvz
r_xvf
az
b_az
reloc
f_type

Earthquake rupture table

evid
datetime
lat
lon
depth
loc_type
loc_grid
mag
mag_type
mag_method
mag_unc
mag_orig
mag_orig_type
mag_orig_unc
ndef
nsta
t_res
reloc
tect_type
tect_method
domain_no
domain_type
strike
dip
rake
aux_strike
aux_dip
aux_rake
f_length
f_width
f_type
z_tor
z_bor

Station magnitude table

magid
evid
net
sta
loc
chan
mag
mag_type
mag_corr
mag_corr_method
amp
amp_peak
amp_trough
amp_max
reloc
SNR
filtered
amp_time

Ground-motion IM tables

gmid
evid
net
sta
loc
chan
component
PGA
PGV
CAV
AI
Ds575
Ds595
MMI
score_mean(x, y, or z)
multi_mean(x, y, or z)
fmin_mean(x, y, or z)
fmax_mean(x, y, or z)
pSA(T)
FAS(f)
clip_prob
clipped

Figure 1. Schematic of the relational setting of six tables within the New Zealand ground-motion database. Bold terms indicate properties that provide relational connectivity between the different tables.

et al., 2009) location methods with the SeisComp3 software suite (Weber et al., 2007). Figure 5a is a histogram of the number of earthquakes by location type. Of these methods, regional centroid moment tensor (CMT) solutions (Ristau, 2013) and LocSAT were used for the greatest number of events (>1800 each), whereas NonLinLoc was been used for the fewest (∼160). The number of located events is primarily dependent on the length of time for which these methods have been used for the GeoNet database. SIMUL (Thurber and Eberhart-Phillips, 1999) is the method used for earthquake relocations, which are discussed further below.

Spatial grids used for earthquake locations are provided in the GeoNet database. These grids vary from 1D global velocity models (iasp91) to 3D NZ-specific velocity models (nz3drx, Eberhart-Phillips et al., 2010). The number of earthquakes located within each of these grids is shown in Figure 5b. The location grid, nz3drx, is used for both the NonLinLoc and SIMUL methods. In total, the 1D location grids for CMT

and iasp91 comprise the majority of event locations. Note that iasp91 and iaspei91 (for which there are only 3 events) are the same models but are recorded in the GeoNet catalog seperately, and thus are preserved this way in the NZGMDB. For the NZGMDB, from 2012 onward, the LocSAT method is used in combination with iasp91 for 1958 events and the NonLinLoc method and relocated events (described subsequently) are used in combination with nz3drx for 985 events.

For a subset of the NZGMDB event locations, earthquake hypocenters have been relocated (Reyners et al., 2011). Over 100,000 relocations were computed for events that occurred from January 2001–March 2010. Although nearly all events in NZ

Figure 2. (a) Distribution of New Zealand earthquakes by tectonic classification (indicated by color). Earthquake magnitude is indicated by the size of the color-filled circles. (b) Map of sites (shown as pink triangles) with high-quality intensity measures used for this database. Note that there are some stations outside of the map area. The color version of this figure is available only in the electronic edition.

during this time period were considered for relocation, earthquakes were excluded from May 2007 to June 2008 and for aftershocks in the first 39 hr following the 2009 M_w 7.8 Dusky Sound earthquake due to incomplete phase picking at the time of publication. The relocated events are indicated by the "reloc" column of Table 1. Figure S1, available in the supplemental material to this article, shows the Euclidian location difference between original and relocated hypocenter locations in the NZGMDB. The lognormal mean and standard deviation of the hypocenter differences are 2.5 and 1.1, respectively. The size of the location differences illustrates that a substantial area for further improvement is to significantly increase the proportion of events in the NZGMDB that have been relocated.

Although true location uncertainties for both the original GeoNet hypocenters and the relocated data are unavailable, Reyners *et al.* (2011) compare the root mean square (rms) arrival-time residuals between both the methods. They found an average reduction of 24% in rms values from the GeoNet hypocenters, which indicates that the 3D velocity structure (Eberhart-Phillips *et al.*, 2010) utilized by Reyners *et al.* (2011) allows for more accurate locations. M_L values in the Reyners *et al.* (2011) relocated catalog were not recalculated and are identical to the values from the original GeoNet hypocenters. For this

database, the local relocated event magnitudes have been corrected with the method described in the Earthquake Magnitude Estimates section.

Earthquake magnitude estimates

Harmonization of magnitude estimates requires the determination of M_w for all events in the NZGMDB. Since 2003, manual calculation of CMT solutions for earthquakes has been undertaken (Herrmann, 2013; Ristau, 2013), with 1881 of those events included in the NZGMDB, of M_w 3.0–8.0. The moment magnitudes and focal mechanisms of this CMT catalog can be considered as practically consistent with respect to variations in adopted computational solutions over time (John Ristau, personal comm., 2023). For events without M_w, we convert available magnitudes to an M_w-equivalent corrected magnitude, when possible.
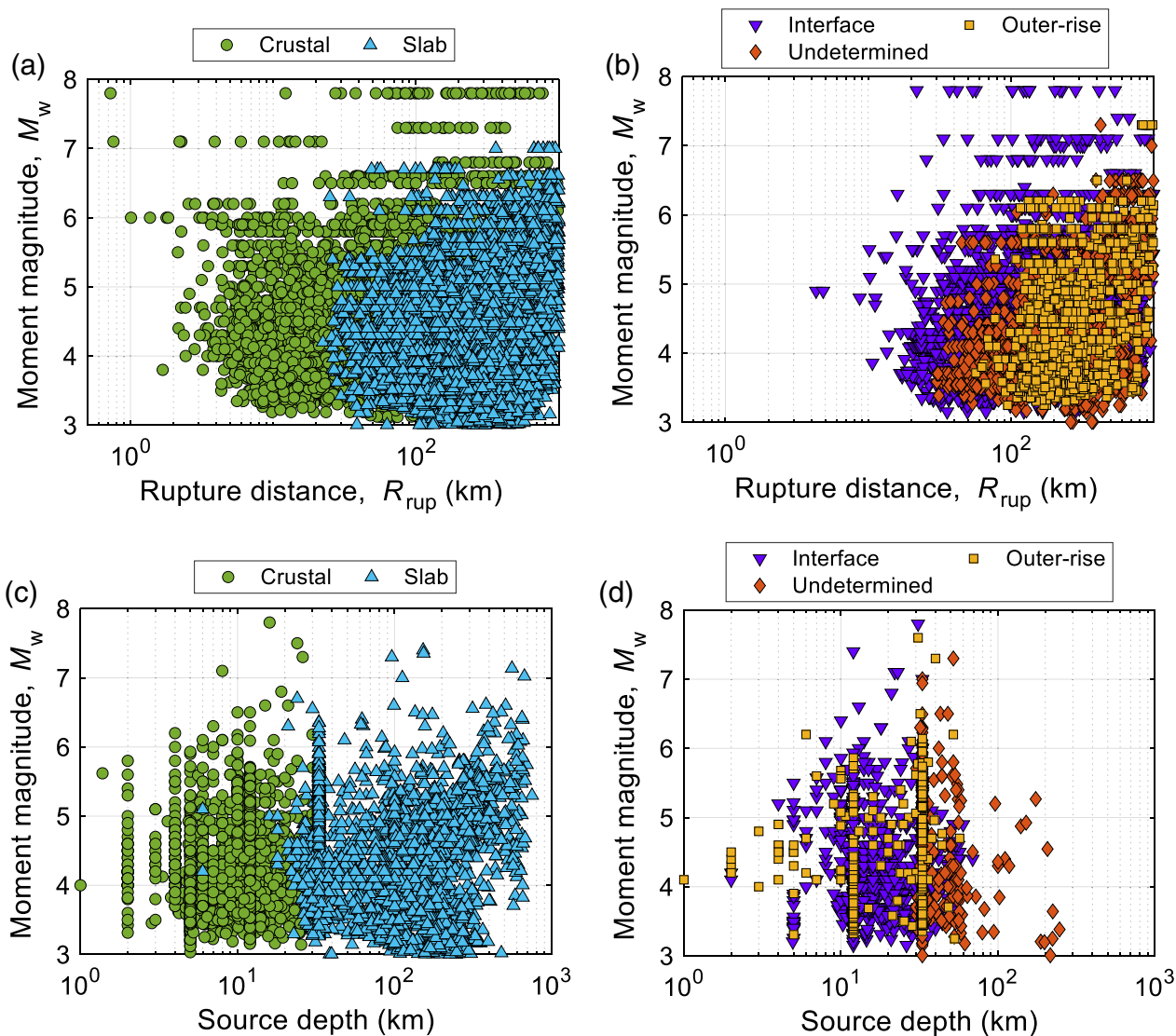
Figure 3. (a,b) Magnitude–distance and (c,d) magnitude–depth distributions of ground motions in the database. The color version of this figure is available only in the electronic edition.
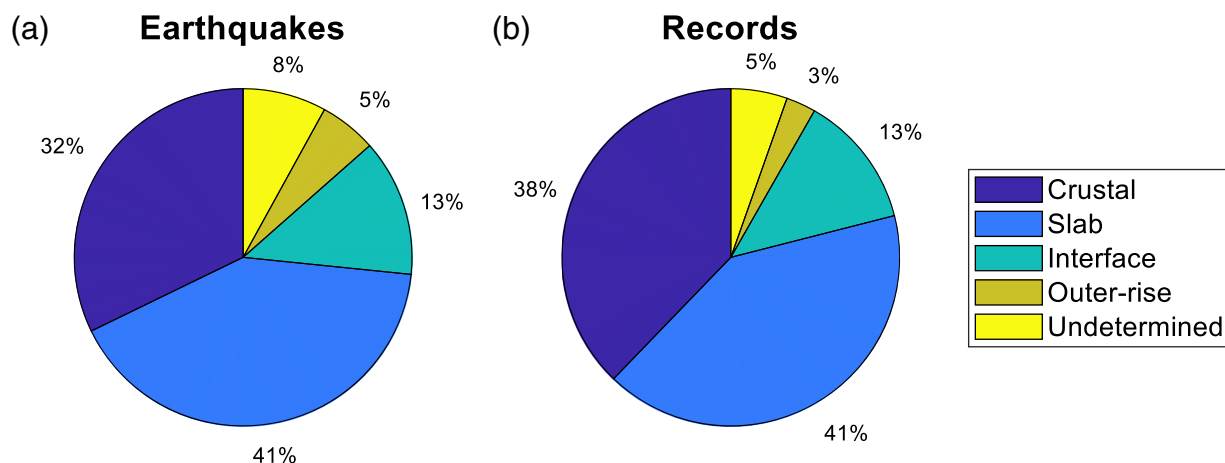
Figure 4. Percentage of (a) events and (b) records by tectonic class. The color version of this figure is available only in the electronic edition.

TABLE 1
Earthquake Rupture Table

Short Name	Full Name	Description
evid	Event identification number	GeoNet event ID
datetime	Event origin time	Date and time are shown as: YEAR:MONTH:DAY HOUR:MIN:SEC UTC
lat	Event origin latitude	Latitude is provided in decimal degrees (°)
lon	Event origin longitude	Longitude is provided in decimal degrees (°)
depth	Event origin depth	Depth is provided in kilometers below sea level
loc_type	Event location method	See the Earthquake Locations section
loc_grid	Event location grid	See the Earthquake Locations section
mag	Event magnitude	Preferred magnitude value according to the scale of mag_type (see the Earthquake Magnitude Estimates section)
mag_type	Event magnitude type	The method used to determine the magnitude, such as local, moment, and so on. M_w is preferred when available
mag_method	Event magnitude method	Magnitude method used to determine the magnitude of the event
mag_unc	Event magnitude uncertainty	Derived from the standard deviation of the station magnitudes
mag_orig	Original event magnitude	Magnitude according to the original value (usually local)
mag_orig_type	Original event magnitude type	The method used to determine the magnitude, such as local, moment, and so on
mag_orig_unc	Original event magnitude uncertainty	Uncertainty as reported for the original event magnitude
ndef	Number of defining phase picks	Used to determine the event hypocenter (latitude, longitude, and depth)
nsta	Number of stations	Used to determine the event hypocenter
nmag	Number of magnitude measures	Used to determine the magnitude of the event
t_res	Event origin time residual	The averaged uncertainty of the predicted origin time provided in seconds (s)
reloc	Relocated	The source of the relocation information. "No" indicates no relocation
tect_class	Event tectonic classification	Options include crustal, interface, slab, outerrise, or undetermined (see the Tectonic Classification section)
tect_method	Tectonic class method	The method used to determine the event tectonic class
domain_no	Tectonic domain number	The number of the tectonic domain in which the event ruptured (see the Tectonic Domain Regionalization section)
domain_type	Tectonic domain type	Dominant tectonic behavior of the domain
strike	Event strike	Strike of the preferred event rupture plane (°) (see the Focal Mechanisms section)
dip	Event dip	Dip of the preferred event rupture plane (°)
rake	Event rake	Rake of the preferred event rupture plane (°)
aux_strike	Event strike	Strike of the auxiliary nodal plane (°)
aux_dip	Event dip	Dip of the auxiliary nodal plane (°)
aux_rake	Event rake	Rake of the auxiliary nodal plane (°)
f_length	Fault rupture length	Along-strike length of the fault rupture plane (km) (see the Finite-Fault Geometry section)
f_width	Fault rupture width	Down-dip width of the fault rupture plane (km)
f_type	Fault rupture type	Method used to determine the fault geometry and kinematics
z_tor	Depth to top of fault rupture	Measured with reference to the ground surface (km)
z_bor	Depth to bottom of fault rupture	Measured with reference to the ground surface (km)

The column labeled "short name" corresponds to the fields found in this table. For several fields, a section name in the description is referenced to provide further information about the field.

The majority of remaining events have M_L estimates that are retrieved from the GeoNet database (GeoNet, 2022a). These magnitudes are adjusted with the equations of Rhoades *et al.* (2021) to more closely represent the M_w unless waveform and/or instrument response information is unavailable. This method uses a newly developed NZ-specific reference attenuation model, which was derived from fitting M_L data to M_w data through regression analysis. The model includes correction terms for attenuation over distance, hypocentral depth, and specific sites.

To recalculate M_L for each station where a phase arrival was detected, we attempted to retrieve instrument response and waveform data. Instrument response and/or waveform data are not always available, especially for events in the early

2000s. For all available components (horizontal and vertical), we calculate the peak displacement amplitude (in millimeters) of the body waves after convolving the seismogram with the response of the Wood–Anderson seismometer (with a gain of 2800, a natural period of 0.8 s, and damping factor of 0.8). Preferably, amplitudes are computed from broadband seismometers. For waveforms with a signal-to-noise ratio (SNR) ≥ 3, the amplitude, hypocentral distance, and depth are used as input to compute the station M_L. Typically, we prefer magnitudes on the vertical component; however, the mean of the two horizontal components is used in rare circumstances when vertical data are corrupt or otherwise unavailable. We determine the inter-quartile range (IQR) of the magnitudes
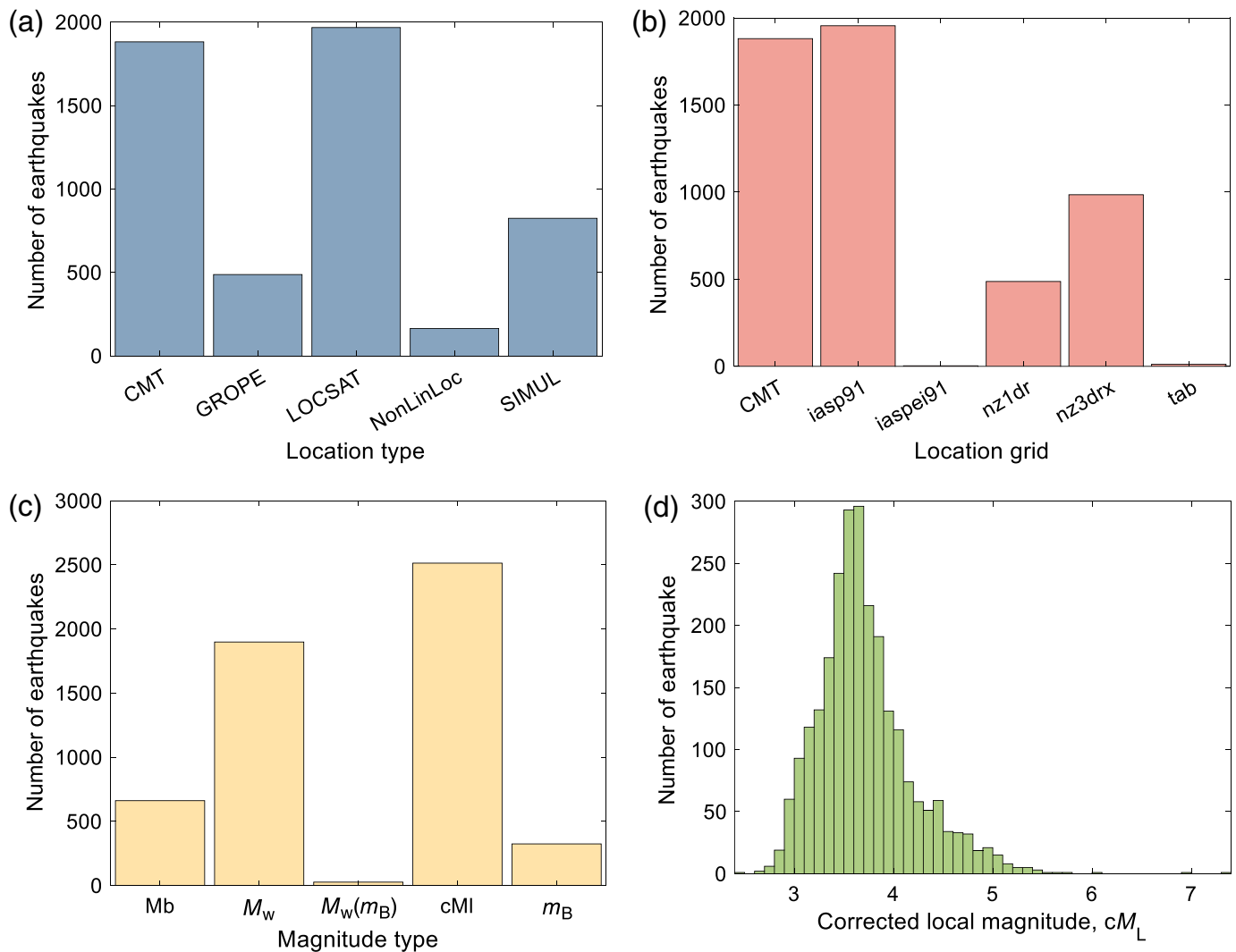
Figure 5. (a) Frequency of different methods used in earthquake locations, (b) frequency of earthquakes by location grid used to locate events, (c) number of earthquakes by magnitude type, and (d) magnitude distribution of corrected local magnitudes (cM_L). The color version of this figure is available only in the electronic edition.

by subtracting the first quantile (Q_1) from the third quantile (Q_3). We then determine the bounds for outlying station magnitudes with the following equations:

$$\text{lowerqe} = Q_1 - 1.5 \times \text{IQR}, \tag{1}$$

$$\text{upperqe} = Q_3 + 1.5 \times \text{IQR}, \tag{2}$$

in which lowerqe and upperqe are the lower and upper bounds for the accepted station M_L, respectively. Finally, the recalculated mean of the station M_L, excluding outliers, is used to determine the cM_L.

From 2012 onward, the GeoNet database (GeoNet, 2022a) provides magnitude results as a summary magnitude, M, which is determined from a mixture of M_L and $M_{(m_B)}$ (estimated M_w based on body-wave magnitude). We believe that combining local and body-wave magnitude measures provides little benefit, as body-wave magnitudes perform as a better estimate on regional scales than local magnitudes. Oftentimes, M_L scales disproportionally on a regional scale, leading to overestimated magnitudes. Fortunately, the GeoNet FDSN web

service (GeoNet, 2022c) provides alternative magnitude measures for events with preferred magnitude types of M. Of these measures, we prefer $M_{(m_B)}$, m_B, or m_B measurements, although they are still not directly equivalent to M_w. If only a M_L value is reported, we perform a cM_L computation.

The number of determined earthquakes by magnitude type is shown in Figure 5c. The bulk of events in the NZGMDB (~2513) have cM_L, whereas M_w and m_B measures comprise most of the remaining data. In some cases, M_L measures could not be corrected due to a lack of available waveform data from the GeoNet FDSN web service. For these values, the M_L–M_w scaling relationship derived from Rhoades *et al.* (2021) can be used; however, such a relationship cannot be applied to relocated hypocenters. In very few cases, cM_L measures could not be determined from vertical seismometer channels, so the

mean of the horizontal channels is reported as cM_{L_H}. The magnitude distribution of cM_L data is shown in Figure 5d.

Tectonic classification

The tectonic classification of an event ("tect_class" field) is determined based on the location of the event relative to various subduction geometry models. Possible classifications include crustal, subduction interface, subduction intraslab, outer rise, and undetermined.

Van Houtte et al. (2017) provided tectonic classifications for the events in their study's database, which considered the proximity of the earthquake's location to subduction interface geometry models, as well as a manual review of focal mechanisms. Therefore, tectonic classifications for those events were adopted for the NZGMDB where available. For events not included in Van Houtte et al. (2017), we utilize two separate subduction zone geometry models, hikpuy and kerpuy. hikpuy uses the Hayes et al. (2018) and Williams et al. (2013) slab geometries for the Puysegur and Hikurangi subduction zones, respectively. Alternatively, kerpuy uses the Hayes et al. (2018) slab geometries for both the subduction zones. The Williams et al. (2013) slab geometry is preferred for determining tectonic class within the Hikurangi subduction zone; however, it covers a smaller geographic region than the Hayes et al. (2018) model, so it cannot always be employed. In those circumstances, we use the Hayes et al. (2018) slab model for Hikurangi. These models have been blended for an optimal slab geometry (Charles Williams via Chris Rollins, personal comm., 2021). The tectonic classification logic follows procedures outlined in Mazzoni et al. (2022) with minor modifications (Dupuis et al., 2023). Figure 2a provides a map plot of earthquake locations categorized by tectonic class.

Tectonic domain regionalization

The domain number of an earthquake ("domain_no" field) corresponds to one of 28 NZ neotectonic domains ("domain_type") in which it occurred (Rattenbury, 2022). These domains are classified based on the dominant fault type (strike-slip, normal, or reverse), which is listed as the domain type, and are used to determine the general fault properties of encompassed earthquakes. The tectonic domain type for each event is shown in Figure S2. Any events outside of the tectonic domains documented in Rattenbury (2022) are considered compressional.

Focal mechanisms

The strike, dip, and rake of an event are determined via a prioritized system with sources specified in the "f_type" field in Table 1. Starting from the highest priority, we first choose strike, dip, and rake from rigorously inverted finite-fault models ("f_type" = "ff," see the Finite-fault geometry section). If rigorously inverted finite-fault models are unavailable, regional CMT solutions (Herrmann, 2013; Ristau, 2013; GeoNet, 2022b), manual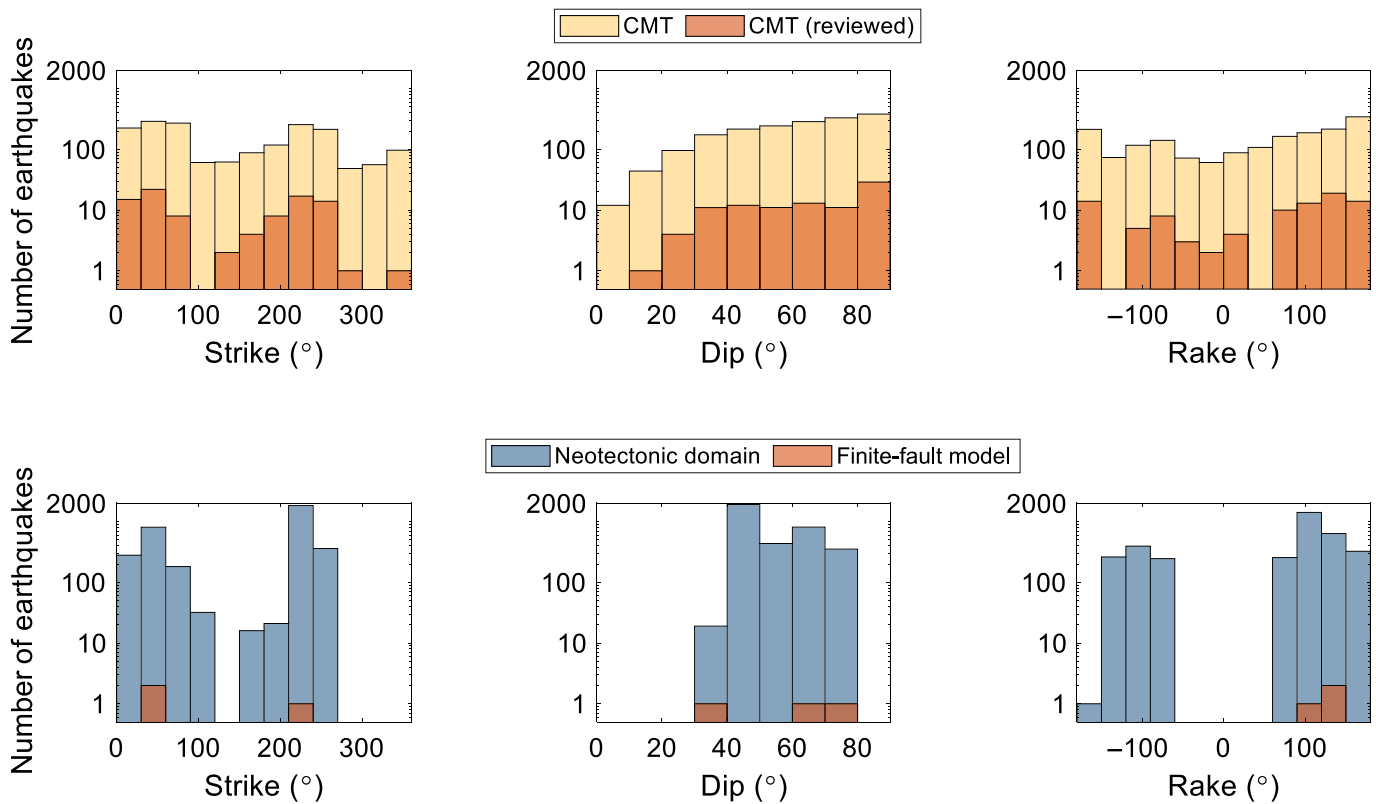ly reviewed by Lee et al. (2021), were used to determine the most likely fault plane ("f_type" = "cmt"). Other regional CMT solutions were compared with their neotectonic domains (Rattenbury, 2022) to find the nearest strike to determine the preferred fault plane ("f_type" = "cmt_unc"). Finally, if none of the above were available, we used average fault orientations from the 28 tectonic domains to determine strike, dip, and rake ("f_type" = "domain"). Any events located outside of the tectonic domains are considered compressional and are assigned a standard strike, dip, and rake of 220°/45°/090°.

Figure 6 shows the distribution of strike, dip, and rake values for finite-fault, CMT, and neotectonic-domain-derived data. CMT-derived values appear to have broader distributions than domain-derived values, particularly in the frequency of dip values. Dominant frequencies are evident in both the examples for strikes of 40° and 220°.

Finite-fault geometry

Finite-fault models that are consistent with those used in ground-motion model development, where available, are used for computing the rupture properties of earthquakes. Currently, the NZGMDB uses finite-fault geometries for three events (with GeoNet event references in parentheses): the 2010 M_w 7.1 Darfield earthquake (publicid: 3366146; Beavan et al., 2010; Bradley, 2012), the 2011 M_w 6.2 Christchurch earthquake (publicid: 3468575; Bradley and Cubrinovski, 2011; Beavan et al., 2011), and the 2016 M_w 7.8 Kaikōura earthquake (publicid: 2016p858000; Bradley et al., 2017; Hamling et al., 2017). For all other events, without event-specific finite-fault models, the along-strike length ("f_length"), down-dip width ("f_width"), depth to the top of the rupture ("z_tor"), and depth to the bottom of the rupture ("z_bor") were computed from scaling relationships (Strasser et al., 2010; Leonard, 2010, 2014; Skarlatoudis et al., 2016) to determine the fault geometry for source–receiver propagation path information.

Along-strike length and down-dip width are computed based on the empirical M_w-scaling relationships of Leonard (2014) and Skarlatoudis et al. (2016) for crustal and subduction interface earthquakes, respectively, based on comparisons of global and NZ-specific studies (Michael Dupuis, personal comm., 2022). First, the rupture areas are calculated using the M_w-area scaling relationships. As M_w-length and M_w-width scaling relationships are available from Leonard (2010), dimensions of crustal earthquakes were proportioned to follow the implied aspect ratio. Skarlatoudis et al. (2016) do not provide M_w-length and M_w-width scaling relations, and hence the length and width are set to be equal (i.e., simply the square root of the area), given that the size of the events requiring such assumptions does not saturate the available rupture widths of the subducting interface zone. Although the Leonard (2010) relationships are for crustal earthquakes, they were also used for slab earthquakes in the NZGMDB v.1.0, because calculations were undertaken before rigorous investigations into slab M_w-scaling relationships, and we found that the alternatives

Figure 6. Frequency of strike, dip, and rake of the preferred rupture plane of earthquakes as a function of determination method—centroid moment tensor (CMT), neotectonic domain, or finite-fault model. The color version of this figure is available only in the electronic edition.

had little impact on calculated lengths and widths (and negligible impacts on subsequently computed source-to-site distances). This update of the NZGMDB v.3.4 adopts the Strasser et al. (2010) M_w-scaling relationships for slab earthquakes from magnitudes 5.9 to 7.8 but retains the dimensions calculated by Leonard (2010) for earthquakes below magnitude 5.9. However, as slab earthquakes are relatively deep, this does not significantly influence any results using the current version of the NZGMDB. For earthquakes with geometry estimated using the M_w-scaling relations, we assume that the hypocenter or centroid location, as described in the relevant earthquake catalog, is located in the middle of the rupture. Therefore, the depth to the top of the rupture is determined by subtracting half of the rupture's vertical height (i.e., vertical distance from the top of the fault to the bottom) from the hypocenter depth, whereas Z_{BOR} is simply the height of the fault added to Z_{TOR}. In cases for which Z_{TOR} from an estimated finite-fault geometry would be reported as a negative depth (i.e., above the ground surface), it is corrected to a value of 0 (i.e., at the ground surface), with the Z_{BOR} value adjusted such that the correct down-dip width is maintained.

It is noted that the prior NZ ground-motion database from Van Houtte et al. (2017) included finite-fault information for 16 events post-2000 (which are in the database documented in this article). For 13 of these events (i.e., excluding the three considered earlier), we concluded that they were not geometries that were consistent with those used in ground-motion model development (i.e., they had geometries that were inconsistent with scaling relations, with many instances of significant zero slip

regions along their outer boundaries). At the present time, due to time constraints, we have not revised these models to be consistent, because the overwhelming majority of observations have source-to-site distances that are not affected by the assumed fault geometries using the scaling-relation-based approach above, which we preferred to use of internally inconsistent event-specific finite faults. This is an obvious area for improvement in the near future.

SITE TABLE

The site table (Table 2) contains basic station information, as well as geotechnical and geophysical site parameter data. A map of all sites used for this database is shown in Figure 2b. The collection and collation of strong-motion site information was undertaken as a parallel workstream by Wotherspoon et al. (2022), which the reader is directed to for more comprehensive details. Here, we focus on a summary of the site characterization information that is of direct relevance for ground-motion modeling.

Time-averaged shear-wave velocity over the top 30 m of the ground profile (V_{S30}), site fundamental period (T_0), depths to 1.0 and 2.5 km/s shear-wave velocity horizons ($Z_{1.0}$ and $Z_{2.5}$, respectively), and other site data compiled in Wotherspoon

TABLE 2
Site Table Information Adopted from Wotherspoon et al. (2022)

Short Name	Full Name	Description
net	Site network name	Seismograph network of site
sta	Site station name	Instrument station name
lat	Site latitude	Latitude of the site in decimal degrees
lon	Site longitude	Longitude of the site in decimal degrees
elev	Site elevation	Elevation of the site above sea level in meters
site_class	Site classification	Site classification is based on the NZS1170.5 site subsoil class approach (A–E; New Zealand Standards, 2004)
V_{S30}	V_{S30} value	Time-averaged shear-wave velocity of the top 30 m (m/s)
V_{S30}_std	–	Standard deviation of V_{S30}. All standard deviations in this table are in sigma of the natural log of the metric
Q_V_{S30}	–	Quality rating of V_{S30} measurement, ranging from 1 (well-constrained) to 3 (poorly constrained)
V_{S30}_ref	–	V_{S30} source reference
$T0$	Site period	Fundamental site period (s)
$T0$_std	–	Standard deviation of the fundamental site period (s)
Q_$T0$	–	Quality rating of $T0$ measurement
D_$T0$	–	Method for determining site period
$T0$_ref	–	$T0$ source reference
Z1.0	1.0 km/s shear velocity depth	Depth (in m) to shear-wave velocities of 1.0 km/s
Z2.5	2.5 km/s shear velocity depth	Depth (in km) to shear-wave velocities of 2.5 km/s
Z1.0_std	–	Standard deviation of Z1.0 (m)
Z2.5_std	–	Standard deviation of Z2.5 (km)
Q_Z1.0	–	Quality rating of Z1.0 measurement
Q_Z2.5	–	Quality rating of Z2.5 measurement
Z1.0_ref	–	Z1.0 source reference
Z2.5_ref	–	Z2.5 source reference
site_domain_no	Site domain number	Number of the tectonic domain the site is located within
basin	Underlying basin	Name of the modeled NZVM basin underlying the site

The column labeled "short name" corresponds to the fields found in the site table. The "full name" of the field is listed in the next column, followed by a "description" providing further explanation of the field and units of measurement, where applicable.

et al. (2022) are drawn from several sources. Data are prioritized based on a heuristic quality metric, Q1–Q3 with Q1 denoting the highest quality (Kaiser, Van Houtte, et al., 2017; Wotherspoon et al., 2022), and the source references are reported in the *_ref category for each site parameter. Distributions of V_{S30} and $Z_{1.0}$ values (the most common primary and secondary site parameters in empirical ground-motion modeling, respectively) for NZ stations are illustrated in Figure 7, with histograms for both measured (Q1) and inferred (Q2 and Q3) data.

PROPAGATION PATH TABLE

The propagation path table (Table 3) contains source–receiver information, such as source-to-site distance and azimuth. Several measures of source-to-site distance are included: R_{epi}, R_{hyp}, R_{JB}, R_{rup}, R_x, R_y, R_{TVZ}, and R_{XVF}, which are described in Table 3.

The propagation path table includes seven different source-to-site distance measures. R_{epi} and R_{hyp} are the epicentral and hypocentral distances (in kilometers) from the event to the instrument station. Both R_{JB} and R_{rup} depend on the fault

geometry of the earthquake, which was described in the Finite-Fault Geometry section. R_{JB} is the shortest distance (in kilometers) to the surface projection of the rupture plane. R_{rup} is the shortest distance (in kilometers) to the rupture plane. R_x is the horizontal distance (in kilometers) from the top edge of the rupture measured perpendicular to the fault strike. R_y is the horizontal distance (in kilometers) from the center of the rupture measured parallel to the fault strike.

R_{TVZ} is the decimal fraction of R_{epi} that traveled through the Taupō volcanic zone (TVZ). The polygon used to define the TVZ dimensions is derived from neotectonic domain 4 (Havre trough–Taupō rift). R_{TVZ} is included because the TVZ is known to have higher anelastic attenuation than the surrounding crust, which affects recorded ground motions (e.g., McVerry et al., 2006). This value is reported from 0 (none of the paths is within the TVZ) to 1 (the entire path is within the TVZ). As an example, Figure 8 illustrates the propagation path of event 1597193 to station WCDS through the TVZ, which has a reported value of 0.490. R_{XVF} is the Euclidean distance (in kilometers) from the intersection of R_{epi} with the TVZ to the seismic station; the value of the path shown is
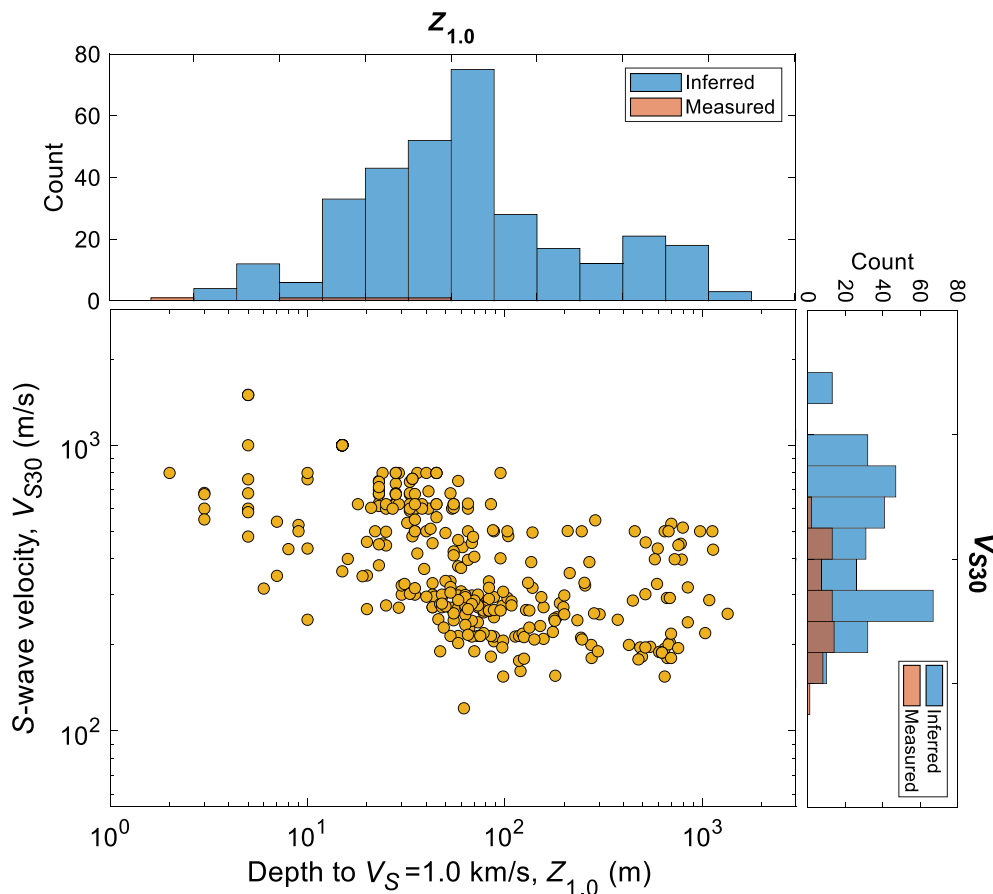
Figure 7. $Z_{1.0}$ and V_{S30} distributions at recording sites. The color version of this figure is available only in the electronic edition.

44.71 km. This is illustrated as the blue portion of the path in Figure 8. If the station is within the TVZ, the value is set to 0, whereas cases with no such intersection have a reported null value.

STATION MAGNITUDE AND PHASE ARRIVAL TABLES

The station magnitude table (Table 4) provides additional detail that underpins the M_w values in the earthquake rupture table. The motivation for this separate table results from the recognition that many events contain only uncorrected M_L, and this table provides a basis for improved magnitude estimates through event relocations, cM_L estimates, and potentially new direct M_w estimates. The station magnitude table contains both M_L and cM_L for source–receiver pairs. Magnitude values are provided from the original GeoNet

---

TABLE 3
Propagation Path Table Information

Short Name	Full Name	Description
evid	Event identification number	Identification number associated with the source earthquake
net	Site network name	Seismograph network of site
sta	Site station name	Instrument station name
r_epi	Epicentral distance	
r_hyp	Hypocentral distance	
r_jb	Joyner–Boore distance	
r_rup	Rupture distance	Measured in kilometers.
r_x	Strike-perpendicular distance	
r_y	Strike-parallel distance	
r_tvz	Taupō volcanic zone distance	The decimal fraction of R_{epi} that traveled through the Taupō volcanic zone (TVZ)
r_xvf	Station to TVZ distance	Euclidean distance, measured in kilometers, from the intersection of the epicentral path with the TVZ to the seismic station. If the station is within the TVZ, the value is set to 0. If there is not an intersection of the propagation path with the TVZ, the value is null
az	Site-source azimuth	Azimuth, in decimal degrees, from the observing site to the earthquake source
b_az	Source-site azimuth	Azimuth, in decimal degrees, from the earthquake source to the observing site
reloc	Relocated	The source of the relocation information. "No" indicates no relocation
f_type	Fault rupture type	Method used to determine the fault properties (strike, dip, rake, length, and width). See the Finite-fault Geometry section

The column labeled "short name" corresponds to the fields found in the propagation path table. The "full name" of the field is listed in the next column, followed by a "description" providing further explanation of the field and units of measurement, where applicable. For several fields, a section label in the description is referenced to provide further information about the field.
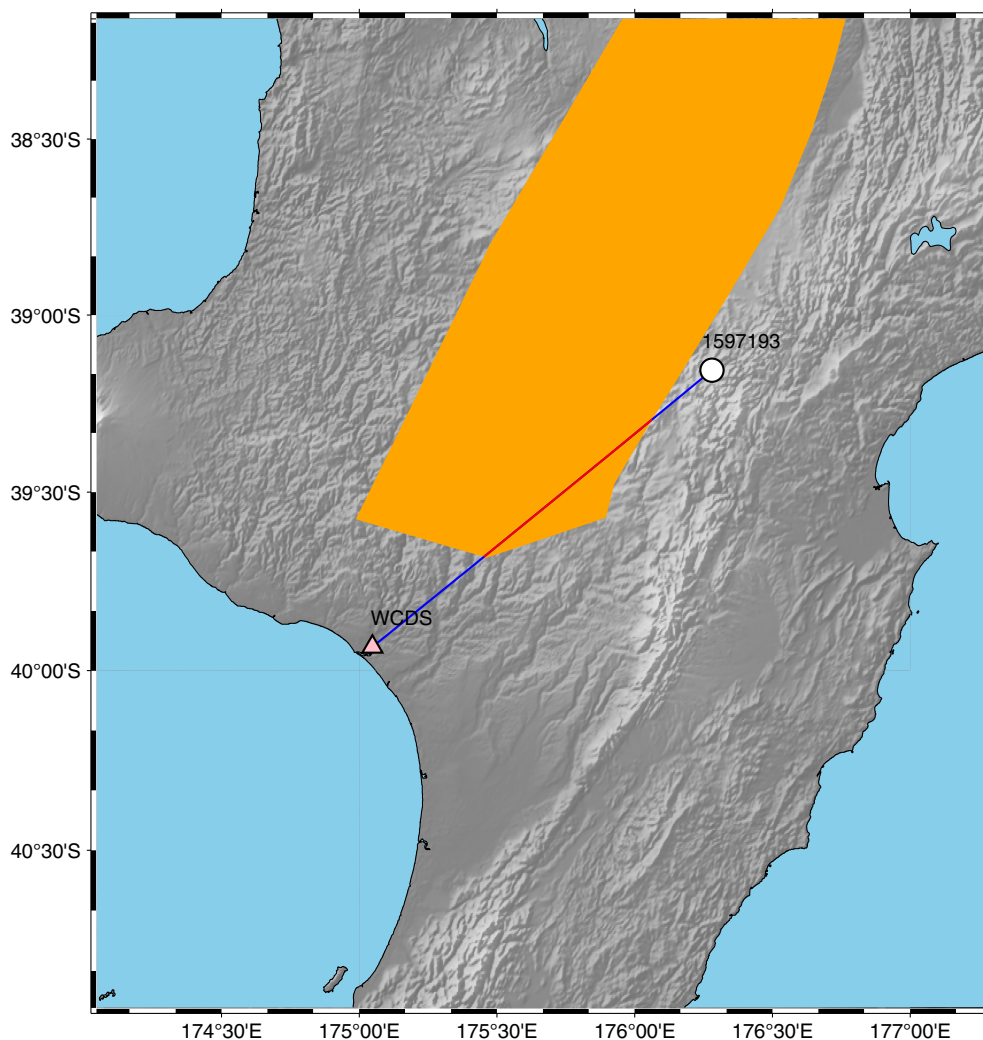
Figure 8. Map showing the R_{TVZ} path for event 1597193 to station WCDS. The Taupō volcanic zone (TVZ) is represented by the orange shape overlying the North Island. The blue line is the portion of the path outside of the TVZ; the red line is the portion of the path within the TVZ. The color version of this figure is available only in the electronic edition.

structure, and SH/SV and P waveform amplitudes. This information can be used for the computation of focal mechanism solutions.

GROUND-MOTION IM TABLE

The ground-motion IM table (Table 6) provides IMs for each event at each station having recorded data. IMs include peak ground acceleration (PGA), peak ground velocity (PGV), and 5%-damped pseudospectral accelerations (pSA) at 31 vibration periods ranging from $T = 0.01$–10 s, Fourier amplitude spectra (FAS) from 0.1 to 100 Hz, and other IMs as discussed in the Ground-motion IMs section.

Computed IMs are provided for three orthogonal components (000, 090, ver), as well as the orientation-independent 50th percentile (median) and 100th percentile (maximum) across all possible azimuths in the horizontal plane, RotD50, and RotD100 (Boore, 2010), respectively. The following sections provide the specifics of ground-motion extraction, processing, and IM computation.

database (mag, GeoNet, 2022a), as well as for the cM_{L} ("mag_-corr"). See the Earthquake Magnitude Estimates section for details on the procedure used to correct M_{L} to be analogous to M_{w}. Because the release of the NZGMDB v.1.0, the "SNR," "filtered," and "amp_time" fields have been added. "SNR" is the velocity time-domain SNR of the earthquake. "filtered" indicates whether a high-pass filter of 1 Hz was used via ObsPy. For filtered data, we correct for the gain of the filter using the iirfilter and sosfreqz functions from scipy. "amp_time" indicates the UTC datetime where the peak amplitude is measured. These fields can help to provide metrics for filtering and quality control.

The phase arrival table (Table 5) includes information about earthquake phases that are associated with located earthquakes. It is our intention to expand on this table with first-motion information (compressional, dilatational, or indeterminate), take-off angles as determined within a 3D velocity

Ground-motion extraction

Ground-motion waveforms were extracted for analysis from the GeoNet FDSN web service (GeoNet, 2022c; see Data and Resources). Data were acquired from stations with detected arrivals and/or within a radius of the hypocenter based on the magnitude–distance scaling relationship shown in Figure S3. This relationship was established by determining the R_{rup} corresponding to PGV thresholds based on the Bradley (2013) empirical ground-motion model. Although PGV thresholds were initially chosen to correspond to shaking levels of interest for ground-motion modeling studies, this resulted in distances that we considered were too small for smaller M_{w} earthquakes. Therefore, variable M_{w}-dependent PGV thresholds were heuristically determined and corresponding M_{w}-dependent R_{rup} were calculated. Finally, the search radius used is the double of the calculated R_{rup} for each M_{w} to

TABLE 4
Station Magnitude Table Information

Short Name	Long Name	Description
magid	Magnitude identification number	The magid is notated as the evid followed by an "m" and an index for the number out of the total station magnitudes for that event, for example, 1503993m13
net	Site network name	Seismograph network of site
sta	Site station name	Instrument station name
loc	Site location name	Indicates the recording instrument at the site
chan	Site channel	Denotes the site channel used to measure amplitude and calculate station magnitude
evid	Event identification number	Identification number associated with the source earthquake
mag	Event magnitude	Uncorrected magnitude. See the Earthquake Magnitude Estimates section
mag_type	Event magnitude type	Magnitude type of the uncorrected magnitude. See the Earthquake Magnitude Estimates section
mag_corr	Event corrected magnitude	Corrected local magnitude. See the Earthquake Magnitude Estimates section
mag_corr_method	Event magnitude correction method	Method used to correct local magnitude (Rhoades et al., 2021). See the Earthquake Magnitude Estimates section
amp	Preferred amplitude measure	Set as the maximum amplitude of the signal in microns by default, convolved with the Wood–Anderson response. See the Earthquake Magnitude Estimates section
amp_peak	Peak amplitude	Largest positive amplitude of the signal in microns, convolved with the Wood–Anderson response
amp_trough	Trough amplitude	Largest negative amplitude of the signal in microns, convolved with the Wood–Anderson response
amp_max	Absolute amplitude	Highest amplitude determined from the absolute value of the peak and trough values in microns, converted to Wood–Anderson response
reloc	Relocated	The source of the relocation information. "No" indicates no relocation
SNR	Signal-to-noise ratio	The ratio of the maximum amplitude to the peak noise
filtered	High-pass filter	Indicates whether or not a high-pass filter was necessary to attain an SNR ≥ 3 for
amp_time	Maximum amplitude datetime	The datetime of the measured maximum amplitude

The column labeled "short name" corresponds to the fields found in the station magnitude table. The "full name" of the field is listed in the next column, followed by a "description" providing further explanation of the field and the units of measurement, where applicable. For several fields, a section in the description is referenced to provide further information about the field.

TABLE 5
Phase Arrival Table Information

Short Name	Long Name	Description
arid	Arrival identification number	The arid is notated as the event identification number, followed by an "a" and the index for the number out of the total station arrivals for that event, for example, 1503993a13
datetime	Phase arrival time	Date and time are shown as YEAR:MONTH:DAY HOUR:MIN:SEC UTC
net	Site network name	Seismograph network of site
sta	Site station name	Instrument station name
loc	Site location name	Indicates the recording instrument at the site
chan	Site channel	Denotes the site channel of the associated phase arrival
phase	Phase arrival name	Name of the phase arrival (e.g., P or S phases)
t_res	Arrival-time residual	The arrival-time residual is the time difference between the observed and predicted arrival times in seconds (s)
evid	Event identification number	Identification number associated with the source earthquake

The column labeled "short name" corresponds to the fields found in the phase arrival table. The "full name" of the field is listed in the next column, followed by a "description" providing further explanation of the field and the units of measurement, where applicable.

conservatively obtain more ground motions if available. This follows a philosophy of obtaining more than typically needed, as the user of the NZGMDB should apply their own acceptable distance criteria for their specific application.

Waveforms are downloaded for all possible channels for both accelerometers and seismometers to miniSEED files (miniSEED, 2012). The time window t_{win} in seconds is determined with the following equation:

$$t_{\mathrm{win}} = (S_{\mathrm{arr}} + 1.2 \times D_{s595}) - (P_{\mathrm{arr}} - 15), \tag{3}$$

in which P_{arr} is the P arrival time, and S_{arr} is the S arrival time. The D_{s595} value is determined with a modified version of the

TABLE 6
Ground-Motion Intensity Measure Table Information

Short Name	Long Name	Description
gmid	Ground-motion identification number	The gmid is notated as the event identification number, followed by "gm" and the index for the number out of the total ground motions for that event, for example, 1519274gm54
evid	Event identification number	Identification number associated with the source earthquake
net	Site network name	Seismograph network of site
sta	Site station name	Instrument station name
loc	Site location name	Indicates the recording instrument at the site
chan	Site channel	Denotes the first two letters of the site channel of the ground motion
component	Ground-motion component	Denotes the component used to compute intensity measures, which can be 000, 090, ver, rotd50, or rotd100
PGA	Peak ground acceleration	Measured in g
PGV	Peak ground velocity	Measured in cm/s
CAV	Cumulative absolute velocity	Measured in g-s
I_A	Arias intensity	Measured in m/s
D_{s575}	5%–75% significant duration	Duration of shaking between 5% and 95% accumulation of Arias intensity (s)
D_{s595}	5%–95% significant duration	Duration of shaking between 5% and 75% accumulation of Arias intensity (s)
MMI	Modified Mercalli intensity	Intensity scale measured from 1.0 (not felt) to 12.0 (extreme) (Worden *et al.*, 2012)
score_mean_(X, Y, Z)	Classification score	Mean quality score (generally 0–1) of the ground motion for 090, 000, and Z channels. Verticals not provided in RotD50 and RotD100 tables
f_min_mean_(X, Y, Z)	Minimum frequency	Mean minimum viable frequency (Hz) of the ground motion for 090, 000, and Z channels. Verticals not provided in RotD50 and RotD100 tables
f_max_mean_(X, Y, Z)	Maximum frequency	Mean maximum viable frequency (Hz) of the ground motion for 090, 000, and Z channels. Verticals not provided in RotD50 and RotD100 tables
multi_mean_(X, Y, Z)	Multiple score	Mean multiple score (generally 0–1) of the ground motion for 090, 000, and Z channels. Verticals not provided in RotD50 and RotD100 tables
pSA(T)	Pseudoacceleration response spectra	Measured in g for various periods denoted by _period, for example, pSA_1.0. See the Ground-Motion Intensity Measures section
FAS(f)	Fourier amplitude spectra	Measured in g for various frequencies denoted by _frequency, for example, FAS_1.0. See the Ground-motion IMs section

The column labeled "short name" corresponds to the fields found in the ground-motion intensity measure table. The "full name" of the field is listed in the next column, followed by a "description" that provides further explanation of the field and units of measurement, where applicable. For several fields, a section number in the description is referenced to provide further information about the field.

equations of Afshari and Stewart (2016), as described subsequently. An additional term (F_D) was added for earthquakes with M_w greater than 5.0 to compensate for increasingly longer wave trains observed in NZ with distance (R) and magnitude (M):

$$F_D = (0.124 \times R + 20.46) \times (M - 5), \qquad (4)$$

which modifies equation (2) of Afshari and Stewart (2016):

$$\ln D_s = \ln(F_E + F_P + F_D) + F_S, \qquad (5)$$

in which D_S is the significant duration of shaking, F_E and F_P are the earthquake source and path duration terms, and F_S is a site term. F_D is estimated from empirical observation from several NZ events, including the 2016 Kaikōura, 2011 Christchurch, and 2009 Dusky Sound earthquakes, among others.

Ground-motion classifications
No further preprocessing steps are performed before classifying the quality of the waveforms. Waveform records are selected for extraction and classification based on several factors.

1. The event magnitude as reported by GeoNet is equal to or exceeds the magnitude threshold (currently 4.0).
2. Station metadata (latitude, longitude, and elevation) are available for the recording instrument.
3. If a station has multiple recording instruments, high sample-rate accelerometers are preferred (HN, 80–200 Hz), followed by lower sample-rate accelerometers (BN, 50 Hz). In the future versions of the GMDB for which other instrument channels will be included, their inclusion within this hierarchy will be given due consideration.
4. Instrument response for the given instrument and time period is available.

The quality of the data is assessed with a ground-motion classification (GMC) neural network (Dupuis *et al.*, 2023), which is a deep learning-based model specifically developed for predicting the quality of each individual component of ground motions in NZ. For training input, the waveform record quality score was manually labeled based on the percentage of pre-event noise to the PGA value, the amount of the

waveform coda captured, any instrument malfunctions, and the presence of phases from multiple earthquakes within single records. Additional quality criteria are discussed in Dupuis et al. (2023). From these criteria, a quality score of 0–1 was given to the records, with 0 indicating the lowest quality and 1 the best quality. The labeled quality scores for the model development are at discrete values (i.e., either 0, 0.25, 0.5, 0.75, or 1.0), given the difficulty in providing more accuracy in the quality labeling. GMC gives mean predictions of quality score on a continuous scale (0–1).

Besides the quality score, GMC was also trained to predict the minimum usable frequency ("f_{min}") and the probability of a record containing multiple events. f_{min} was first labeled on a scale of 0.01–10 Hz based on the amount of noise contamination, the spectral SNR (i.e., SNR ≳ 2), and other Fourier amplitude characteristics such as low-frequency slope. The signal is considered to be the part of the record after the P arrival, and the noise (typically 15 s) is the portion before P arrival. Spectral SNR was computed as the smoothed FAS of the signal divided by that of the noise. GMC f_{min} predictions are on a continuous scale between 0.01 and 10.0 Hz. Further, GMC also gives a probability scale for whether records may contain multiple events, ranging from 0 (no more than one event) to 1 (exceedingly likely that there is more than one event). Although not predicted by the GMC, the maximum usable frequency (f_{max}) is determined as the minimum value between the highest frequency with SNR > 3 and 80% of the Nyquist frequency.

In addition, we identify potentially clipped records using the "clipping_ann" function of the "gmprocess" module (Hearne et al., 2019). In the flatfiles, we provide a probability ("clip_prob") from 0 to 1, on whether the data are potentially clipped and flag any data with a "clip_prob" value higher than 0.2 (true). In certain cases, the neural network (Bellagamba et al., 2019) fails to classify waveforms, and the "clipped" and "clip_prob" fields are filled with null values.

Finally, we proceed with records passing the following additional screening: (1) only strong-motion sensors (HN and BN channels, as further discussed in the Verification of accelerometer versus seismometer data section); (2) event depth < 500 km; (3) rupture distance R_{rup} < 1000 km; (4) quality score (X, Y, Z) > 0.5; (5) f_{min} (X, Y, Z) < 2 Hz; (6) f_{max} (X, Y, Z) > 4 Hz; (7) probability of multiple events (X, Y, Z) < 0.2; and (8) clip_prob (X, Y, Z) < 0.2.

Ground-motion preprocessing

The prioritized data determined via the GMC neural network and other criteria are preprocessed before calculation of IMs. Preprocessing is performed almost entirely with the ObsPy Python suite (Beyreuther et al., 2010; Krischer et al., 2015) and is modeled after the procedures of Van Houtte et al. (2017). Waveforms are first demeaned, detrended, padded with the first and last values to the beginning and the end, respectively, and then tapered. Padding the data helps to

eliminate anomalous spikes caused by instrument response removal and filtering. Instrument sensitivity is removed in the frequency domain via ObsPy, and any waveforms measured in velocity are differentiated to acceleration. The three components are rotated to the ZNE orientation, and the zero-pads are trimmed. The units of acceleration are converted to units of gravity ($g = 9.810$ m/s^2). A high-pass Butterworth filter with a corner frequency of 0.05 Hz with four filter corners is applied in the frequency domain to minimize very long-period noise while preserving as much of the signal as possible. We tested this method with shorter (seconds) and longer (minutes) records to ensure that no anomalous spikes were generated at the beginning or end of the waveforms from the filtering process after trimming the data. Finally, the data are output to ASCII formatted text files.

Ground-motion IMs

Preprocessed data are used as input to calculate IMs. IMs are computed for 000 (NS), 090 (EW), and vertical (Z) components, as well as the RotD50 and RotD100. pSAs are calculated for 31 periods of 0.01, 0.02, 0.03, 0.04, 0.05, 0.075, 0.1, 0.12, 0.15, 0.17, 0.2, 0.25, 0.3, 0.4, 0.5, 0.6, 0.7, 0.75, 0.8, 0.9, 1.0, 1.25, 1.5, 2.0, 2.5, 3.0, 4.0, 5.0, 6.0, 7.5, and 10.0 s. FAS are computed for 100 frequencies logarithmically spaced from 0.1 to 100.0 Hz. Further IMs include PGA, PGV, cumulative absolute velocity (CAV), Arias intensity (I_A), D_{s575} (5%–75% significant duration), D_{s595} (5%–95% significant duration), and modified Mercalli intensity (MMI). Although pSA has been calculated for up to 10.0 s vibration period for all records, this does not imply that the long period pSA are all usable. The predicted minimum usable frequencies from the GMC must also be considered when determining the maximum vibration period that is usable for each application.

The numbers of records per event and per station are shown in Figure 9a,b, respectively. From years 2000 to 2022, the number of records gradually increases (Fig. 9c), and this coincides with increased availability of waveform data and the addition of new stations to the NZ network. The year 2016 contains an anomalously high number of records due to the Kaikōura earthquake sequence.

FLATFILES

For the convenience of the users of the NZGMDB, we have provided flatfiles of the ground-motion IM tables (Table 7). The flatfiles provide event, site, path metadata, and IMs, and are discussed in the sections indicated in the "Description" column. Flatfiles are provided for five ground-motion components, 000, 090, vertical, RotD50, and RotD100.

DISCUSSION
Earthquake locations and focal mechanism solutions
As earthquake locations are reviewed, we intend to improve the catalog by relocating all events possible using a new application
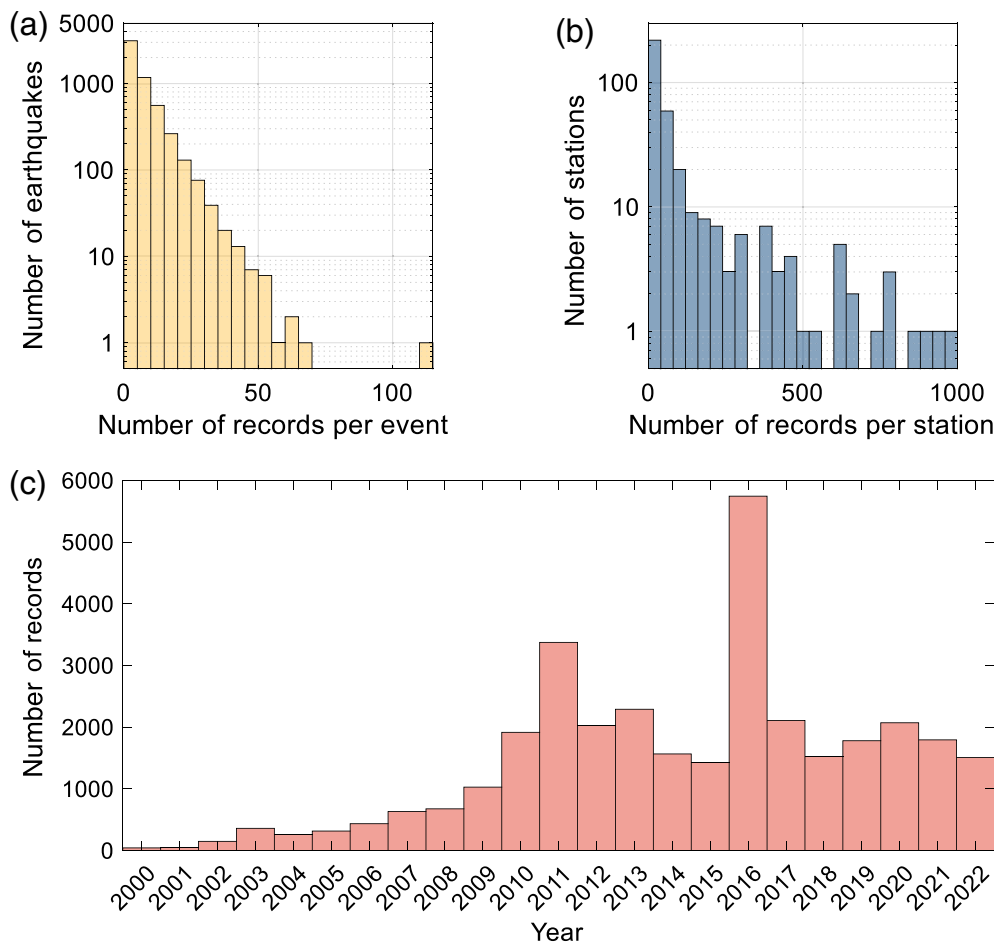
Figure 9. Frequency of observations (a) per event, (b) per station, and (c) number of ground-motion records by year. The color version of this figure is available only in the electronic edition.

A large percentage of the GeoNet database is comprised of events without regional CMT or focal mechanism solutions (GeoNet, 2022a). This percentage is even larger for earthquakes that were not included in the NZGMDB. Computing the best estimate focal mechanism solutions for events will help to better determine earthquake rupture properties rather than relying on the fault properties of the encompassing neotectonic domain. We can use the deep learning approach of Ross et al. (2018) to automatically determine the polarities of P arrivals. In combination with the S/P amplitude ratios, the P polarities are used as input with the focal mechanism determination program HASH (Hardebeck and Shearer, 2002, 2003). We have developed a functional implementation of these methods and intend to update the NZGMDB with these results in the future version.

of the maximum intersection (MAXI) method (Font et al., 2004) and the recent New-Zealand-wide 3D velocity model (Eberhart-Phillips et al., 2020). The efficacy of this method and the robustness of the results will be compared to other proven methods, such as SIMUL (Thurber and Eberhart-Phillips, 1999), NonLinLoc (Lomax et al., 2009), and hypoTD (Guo and Zhang, 2016).

Metadata uncertainties

Uncertainties in metadata are neither comprehensively quantified or considered in our current version of the NZGMDB, nor other comparable ground-motion databases, for example, NGA-Sub (Mazzoni et al., 2022). For instance, uncertainties in earthquake location and faulting parameters are not provided, because this information is often unavailable through GeoNet.

TABLE 7
Columns Provided in the Ground-Motion Intensity Measure Flat Files

Data Source	Column Names	Description
Event metadata	ev_lat, ev_lon, ev_depth, mag, mag_type, tect_class, domain_no, domain_type, strike, dip, rake, f_length, f_width, f_type, z_tor, z_bor, reloc	See Table 1
Site metadata	V_{S30}, V_{S30}_std, Q_V_{S30}, $T0$, $T0$_std, Q_$T0$, Z1.0, Z1.0_std, Q_Z1.0, Z2.5, Z2.5_std, Q_Z2.5, site_domain_no	See Table 2
Propagation path metadata	r_epi, r_hyp, r_jb, r_rup, r_tvz, r_xvf	See Table 3
Clipping metadata	clipped, clip_prob	See the Verification of accelerometer versus seismometer data section

The data source indicates the source table within the database for the metadata included in the flat file. "Column names" are the specific data pulled from the data source. The description indicates the section where additional information about these data can be found.

In addition to earthquake location and faulting parameters, magnitude uncertainty is given for cM_L and estimated by propagating the method uncertainty of Rhoades *et al.* (2021) with the standard deviation of station magnitudes. This accounts for 37% of events. For the remaining events with a direct M_w from CMT or m_B, uncertainty is not quantified due to the lack of relevant information from GeoNet. For site metadata, a heuristic quality metric, Q1–Q3 (Kaiser, Van Houtte, *et al.*, 2017; Wotherspoon *et al.*, 2022), is assigned for each site parameter.

Uncertainty quantification for metadata in ground-motion databases represents a clear area for improvement. For instance, location uncertainty can potentially be estimated based on the rms of the arrival times. The previously noted MAXI-3D method (Font *et al.*, 2004) performs uncertainty estimations by computing the statistical significance of nearby nodes to the maximum intersection using the F-test (also known as Harley's test) to produce uncertainty clouds. One can also compute the best-fit error ellipses to the uncertainty clouds in the *X-Y* direction and calculate the standard deviation in the *Z* direction. Currently, we have tested this method for the years 2000–2022 and are performing a systematic comparison with the original GeoNet hypocenters.

Verification of accelerometer versus seismometer data

Comparison of strong-motion channel HN (high sample-rate accelerometer) with broadband channel HH (high sample-rate seismometer) data helped to identify discrepancies between IMs deconvolved with respect to instrument response for collocated instruments at various stations (GeoNet, 2022d). A collaborative effort was organized with GNS Science to identify and correct these issues. Most of these issues were attributed to the response files used for Obsidian strong-motion dataloggers (see Data and Resources), which have since been corrected. This updated data will be implemented into the future versions of NZGMDB.

Comparison with prior New Zealand database

The prior NZ database, developed by Van Houtte *et al.* (2017), contains 276 events from 1968 to 2016. The NZGMDB developed here is significantly larger, with IMs for 5422 events. Because lower-magnitude data and subsequent years are added to the database, the number of events with high-quality IMs will further expand. Currently, 33,052 three-component records are used to compute high-quality IMs. By comparison, only 4148 high-quality ground-motion recordings were included in the Van Houtte *et al.*, 2017) database.

The NZGMDB expands the number of stations used from 334 to 362. Although Van Houtte *et al.* (2017) includes 219 records before 2000, the NZGMDB includes IMs from the start of 2000 until the end of 2022 but will be expanded with future updates. We have not attempted to process data before 2000

due to the paucity of high-quality waveforms, limited metadata quality, and a general lack of a sufficient number of recordings per event (to constrain event-specific residual terms), but we may do so given time at a future date.

CONCLUSIONS

Our first complete version of the NZGMDB v.1.0, as a part of the 2022 NZ NSHM revision, provided a central database of IMs for events from the GeoNet database with magnitudes approximately greater than 3.0 from the beginning of the year 2000 until 31 December 2020. We have since expanded this catalog to December 2022 in the NZGMDB v.3.4 as well as completely recomputed GMCs, IMs, and corrected magnitudes, while adding additional metrics to the tables for data quality control and filtering. Among many possibilities, these data can be used for evaluating and developing ground-motion models, assessing site conditions, and investigating attenuation and other ground-motion properties.

The NZGMDB has been developed with continuous updates in mind, expanding the date and magnitude range as further processing is performed. In addition, the modular nature of the NZGMDB allows for the inclusion of further data or updates, such as focal mechanism solutions and hypocenter relocations. Finally, we will continue to update the data with the latest information from other sources, such as site information in the site table and recomputed IMs for recalibrated instruments, to maintain an accurate and reliable catalog. We hope to implement the addition of ground motions from the seismometer network, but this requires quality assurance measures before doing so.

DATA AND RESOURCES

The latest version of the New Zealand ground-motion database (NZGMDB) can be accessed and downloaded at https://osf.io/q9yrg/?view_only=05337ba1ebc744fc96b9924de633ca0e (last accessed November 2023). The code used to build the NZGMDB is available at https://github.com/ucgmsim/nzgmdb (last accessed November 2023). Maps in this article were generated with the Python package PyGMT (Uieda *et al.*, 2021), which uses the Generic Mapping Tools (GMT) software package (Wessel *et al.*, 2019). The New Zealand (NZ) earthquake catalog can be accessed using the GeoNet Quake Search tool at https://quakesearch.geonet.org.nz (last accessed January 2023). Ground-motion waveforms were extracted for analysis from the GeoNet International Federation of Digital Seismograph Networks (FDSN) web service available at https://www.geonet.org.nz/data/tools/FDSN (last accessed January 2023). Response files used for Obsidian strong-motion dataloggers can be accessed from https://github.com/GeoNet/help/blob/main/metadata-changes/strongmotion_obsidian4x_response.md (last accessed January 2023). The supplemental figures, which complement this article, are included online as supplemental material.

DECLARATION OF COMPETING INTERESTS

The authors acknowledge that there are no conflicts of interest recorded.

REFERENCES

Afshari, K., and J. P. Stewart (2016). Physically parameterized prediction equations for significant duration in active crustal regions, *Earthq. Spectra* **32,** no. 4, 2057–2081.

Ancheta, T. D., R. B. Darragh, J. P. Stewart, E. Seyhan, W. J. Silva, B. S.-J. Chiou, K. E. Wooddell, R. W. Graves, A. R. Kottke, D. M. Boore, *et al.* (2014). NGA-West2 database, *Earthq. Spectra* **30,** no. 3, 989–1005.

Atkinson, G. (2022). Backbone ground-motion models for crustal, interface and slab earthquakes in New Zealand, *Technical Rept. 2022/48*, GNS Science, doi: 10.21420/QMJ6-P189.

Beavan, J., E. Fielding, M. Motagh, S. Samsonov, and N. Donnelly (2011). Fault location and slip distribution of the 22 February 2011 mw 6.2 Christchurch, New Zealand, earthquake from geodetic data, *Seismol. Res. Lett.* **82,** no. 6, 789–799.

Beavan, J., S. Samsonov, M. Motagh, L. Wallace, S. Ellis, and N. Palmer (2010). The Darfield (Canterbury) earthquake: Geodetic observations and preliminary source model, *Bull. New Zeal. Soc. Earthq. Eng.* **43,** no. 4, 228–235.

Bellagamba, X., R. Lee, and B. A. Bradley (2019). A neural network for automated quality screening of ground motion records from small magnitude earthquakes, *Earthq. Spectra* **35,** no. 4, 1637–1661.

Beyreuther, M., R. Barsch, L. Krischer, T. Megies, Y. Behr, and J. Wassermann (2010). Obspy: A python toolbox for seismology, *Seismol. Res. Lett.* **81,** no. 3, 530–533.

Boore, D. M. (2010). Orientation-independent, nongeometric-mean measures of seismic intensity from two horizontal components of motion, *Bull. Seismol. Soc. Am.* **100,** no. 4, 1830–1835.

Bradley, B. A. (2012). Strong ground motion characteristics observed in the 4 September 2010 Darfield, New Zealand earthquake, *Soil Dynam. Earthq. Eng.* **42,** 32–46.

Bradley, B. A. (2013). A New Zealand-specific pseudospectral acceleration ground-motion prediction equation for active shallow crustal earthquakes based on foreign models, *Bull. Seismol. Soc. Am.* **103,** no. 3, 1801–1822.

Bradley, B., and M. Cubrinovski (2011). Near-source strong ground motions observed in the 22 February 2011 Christchurch earthquake, *Bull. New Zeal. Soc. Earthq. Eng.* **44,** no. 4, 181–194.

Bradley, B., S. Bora, R. Lee, E. Manea, M. Gerstenberger, P. Stafford, G. Atkinson, G. Weatherill, J. Hutchinson, C. de la Torre, *et al.* (2024). The ground-motion characterization model for the 2022 New Zealand National Seismic Hazard Model, *Bull. Seismol. Soc. Am.* doi: 10.1785/0120230170.

Bradley, B. A., S. Bora, R. L. Lee, E. F. Manea, M. C. Gerstenberger, P. J. Stafford, G. M. Atkinson, G. Weatherill, J. Hutchinson, C. A. de la Torre, *et al.* (2022). Summary of the ground-motion characterisation model for the 2022 New Zealand national seismic hazard model, *Technical Rept. 2022/46*, GNS Science, doi: 10.21420/9BMK-ZK64.

Bradley, B. A., H. N. Razafindrakoto, and V. Polak (2017). Ground-motion observations from the 14 November 2016 mw 7.8 kaikōura, New Zealand, earthquake and insights from broadband simulations, *Seismol. Res. Lett.* **88,** no. 3, 740–756.

Bratt, S., and W. Nagy (1991). The locsat program, Science Applications International Corporation, San Diego, California.

Chiou, B., R. Darragh, N. Gregor, and W. Silva (2008). NGA project strong-motion database, *Earthq. Spectra* **24,** no. 1, 23–44.

Dupuis, M., C. Schill, R. Lee, and B. Bradley (2023). A deep-learning-based model for quality assessment of earthquake-induced ground-motion records, *Earthq. Spectra* **39,** no. 4, 2492–2517, doi: 10.1177/87552930231195113.

Eberhart-Phillips, D., S. Bannister, M. Reyners, and S. Henrys (2020). New Zealand wide model 2.2 seismic velocity and qs and qp models for New Zealand, doi: 10.5281/zenodo.3779523.

Eberhart-Phillips, D., M. Reyners, S. Bannister, M. Chadwick, and S. Ellis (2010). Establishing a versatile 3-d seismic velocity model for New Zealand, *Seismol. Res. Lett.* **81,** no. 6, 992–1000.

Font, Y., H. Kao, S. Lallemand, C.-S. Liu, and L.-Y. Chiao (2004). Hypocentre determination offshore of eastern Taiwan using the maximum intersection method, *Geophys. J. Int.* **158,** no. 2, 655–675.

Fry, B., S. Bannister, J. Beavan, L. Bland, B. A. Bradley, S. Cox, J. Cousins, N. Gale, G. Hancox, C. Holden, *et al.* (2010). The M_w 7.6 Dusky Sound earthquake of 2009: Preliminary report, *Bull. N. Z. Soc. Earthq. Eng.* **43,** no. 1, 24–40, doi: 10.5459/bnzsee.43.1.24-40.

GeoNet (2022a). Geonet aotearoa New Zealand earthquake catalogue, doi: 10.21420/0S8P-TZ38.

GeoNet (2022b). Geonet Aotearoa New Zealand earthquake moment tensor solutions, doi: 10.21420/MMJ9-CZ67.

GeoNet (2022c). Geonet Aotearoa New Zealand seismic digital waveform dataset, doi: 10.21420/G19Y-9D40.

GeoNet (2022d). Geonet Aotearoa New Zealand stations metadata repository, doi: 10.21420/0VY2-C144.

Gerstenberger, M., S. Bora, B. Bradley, C. DiCaprio, R. Van Dissen, G. Atkinson, C. Chamberlin, A. Christophersen, K. Clark, G. Coffey, *et al.* (2022). New Zealand National Seismic Hazard Model 2022 revision: Model, hazard and process overview, *Technical Rept. 2022/57*, GNS Science, Lower Hutt, New Zealand, doi: 10.21420/TB83-7X19.

Gerstenberger, M., S. Bora, B. Bradley, C. DiCaprio, A. Kaiser, E. F. Manea, A. Nicol, C. Rollins, M. W. Stirling, K. K. S. Thingbaijam, *et al.* (2024). The 2022 Aotearoa New Zealand National Seismic Hazard Model: Process, overview, and results, *Bull. Seismol. Soc. Am.* doi: 10.1785/0120230182.

Gledhill, K., J. Ristau, M. Reyners, B. Fry, and C. Holden (2011). The darfield (Canterbury, New Zealand) Mw 7.1 earthquake of September 2010: A preliminary seismological report, *Seismol. Res. Lett.* **82,** no. 3, 378–386.

Guo, H., and H. Zhang (2016). Development of double-pair double difference earthquake location algorithm for improving earthquake locations, *Geophys. J. Int.* **208,** no. 1, ggw397, doi: 10.1093/gji/ggw397.

Hamling, I. J., S. Hreinsdóttir, K. Clark, J. Elliott, C. Liang, E. Fielding, N. Litchfield, P. Villamor, L. Wallace, T. J. Wright, et al. (2017). Complex multifault rupture during the 2016 Mw 7.8 Kaikoura earthquake, New Zealand, Science 356, no. 6334, eaam7194, doi: 10.1126/science.aam7194.

Hardebeck, J. L., and P. M. Shearer (2002). A new method for determining first-motion focal mechanisms, Bull. Seismol. Soc. Am. 92, no. 6, 2264–2276.

Hardebeck, J. L., and P. M. Shearer (2003). Using s/p amplitude ratios to constrain the focal mechanisms of small earthquakes, Bull. Seismol. Soc. Am. 93, no. 6, 2434–2444.

Hayes, G. P., G. L. Moore, D. E. Portner, M. Hearne, H. Flamme, M. Furtney, and G. M. Smoczyk (2018). Slab2, a comprehensive subduction zone geometry model, Science 362, no. 6410, 58–61.

Hearne, M., E. Thompson, H. Schovanec, J. Rekoske, B. Aagaard, and C. Worden (2019). USGS automated ground motion processing software, U.S. Geol. Surv. Software Release doi: 10.5066/P9ANQXN3.

Herrmann, R. B. (2013). Computer programs in seismology: An evolving tool for instruction and research, Seismol. Res. Lett. 84, no. 6, 1081–1088.

Hutchinson, J., B. A. Bradley, R. L. Lee, L. M. Wotherspoon, M. Dupuis, C. Schill, J. Motha, A. E. Kaiser, and E. F. Manea (2022). 2021 New Zealand ground-motion database, Technical Rept. 2021/56, GNS Science, Lower Hutt, New Zealand, 45 pp., doi: 10.21420/Z20E-5507.

Johnson, C. (1983). Cusp–automated processing and management for large regional seismic networks, Earthq. Notes 54, 13.

Kaiser, A., N. Balfour, B. Fry, C. Holden, N. Litchfield, M. Gerstenberger, E. D'anastasio, N. Horspool, G. McVerry, J. Ristau, et al. (2017). The 2016 kaikōura, New Zealand, earthquake: Preliminary seismological report, Seismol. Res. Lett. 88, no. 3, 727–739.

Kaiser, A., C. Holden, J. Beavan, D. Beetham, R. Benites, A. Celentano, D. Collett, J. Cousins, M. Cubrinovski, G. Dellow, et al. (2012). The Mw 6.2 Christchurch earthquake of February 2011: Preliminary report, New Zeal. J. Geol. Geophys. 55, no. 1, 67–90.

Kaiser, A., C. Van Houtte, N. Perrin, L. Wotherspoon, and G. McVerry (2017). Site characterisation of geonet stations for the New Zealand strong motion database, Bull. New Zeal. Soc. Earthq. Eng. 50, no. 1, 39–49.

Krischer, L., T. Megies, R. Barsch, M. Beyreuther, T. Lecocq, C. Caudron, and J. Wassermann (2015). Obspy: A bridge for seismology into the scientific python ecosystem, Comput. Sci. Discov. 8, no. 1, 014003, doi: 10.1088/1749-4699/8/1/014003.

Lee, W., and S. Stewart (2018). Large-scale processing and analysis of digital waveform data from the usgs central California microearthquake, in Observatory Seismology: A Centennial Symposium for the Berkeley Seismographic Stations, J. J. Litehiser (Editor), University of California Press, Berkeley, California, 86 pp.

Lee, R. L., B. A. Bradley, E. F. Manea, and J. Hutchinson (2022). Evaluation of empirical ground-motion models for New Zealand application, GNS Science report 2021/61, GNS Science, Lower Hutt, New Zealand, 141 pp., doi: 10.21420/W2M5-YC09.

Lee, R., B. Bradley, E. Manea, J. Hutchinson, and S. Bora (2024). Evaluation of empirical ground-motion models for the 2022 New Zealand National Seismic Hazard Model revision, Bull. Seismol. Soc. Am. doi: 10.1785/0120230180.

Lee, R. L., B. A. Bradley, J. Patterson, J. Motha, and R. W. Graves (2021). Source modelling insights from ground motion simulation

validation of moderate magnitude active shallow crustal earthquakes in New Zealand, Presented at the New Zealand Society for Earthquake Engineering Annual Conference, Christchurch, New Zealand, 8 pp.

Leonard, M. (2010). Earthquake fault scaling: Self-consistent relating of rupture length, width, average displacement, and moment release, Bull. Seismol. Soc. Am. 100, no. 5A, 1971–1988.

Leonard, M. (2014). Self-consistent earthquake fault-scaling relations: Update and extension to stable continental strike-slip faults, Bull. Seismol. Soc. Am. 104, no. 6, 2953–2965.

Lomax, A., A. Michelini, A. Curtis, and R. Meyers (2009). Earthquake location, direct, global-search methods, in Encyclopedia of Complexity and Systems Science, R. A. Meyers (Editor), Vol. 5, Springer, New York, 2449–2473.

Mazzoni, S., T. Kishida, J. P. Stewart, V. Contreras, R. B. Darragh, T. D. Ancheta, B. S. Chiou, W. J. Silva, and Y. Bozorgnia (2022). Relational database used for ground-motion model development in the nga-sub project, Earthq. Spectra 38, no. 2, 1529–1548.

McVerry, G. H., J. X. Zhao, N. A. Abrahamson, and P. G. Somerville (2006). New zealand acceleration response spectrum attenuation relations for crustal and subduction zone earthquakes. Bull. New Zeal. Soc. Earthq. Eng. 39, no. 1, 1–58.

miniSEED (2012). Seed reference manual: Standard for the exchange of earthquake data, Standard, Incorporated Research Institutions for Seismology (IRIS).

New Zealand Standards (2004). Structural design actions - part 5: Earthquake actions - New Zealand, Standard, Standards New Zealand, Wellington, New Zealand, available at https://www.standards.govt.nz/shop/nzs-1170-52004-includes-amdt-1/ (last accessed December 2023).

Rattenbury, M. S. (2022). Regional fault orientation and length analysis, Aotearoa New Zealand, Technical Rept. 2022/13, GNS Science.

Reyners, M., D. Eberhart-Phillips, and S. Bannister (2011). Tracking repeated subduction of the hikurangi plateau beneath New Zealand, Earth Planet. Sci. Lett. 311, nos. 1/2, 165–171.

Rhoades, D. A., A. Christophersen, S. Bourguignon, J. Ristau, and J. Salichon (2021). A depth-dependent local magnitude scale for New Zealand earthquakes consistent with moment magnitude, Bull. Seismol. Soc. Am. 111, no. 2, 1056–1066.

Ristau, J. (2013). Update of regional moment tensor analysis for earthquakes in New Zealand and adjacent offshore regions, Bull. Seismol. Soc. Am. 103, no. 4, 2520–2533.

Ross, Z. E., M.-A. Meier, and E. Hauksson (2018). P wave arrival picking and first-motion polarity determination with deep learning, J. Geophys. Res 123, no. 6, 5120–5129.

Skarlatoudis, A., P. Somerville, and H. Thio (2016). Source-scaling relations of interface subduction earthquakes for strong ground motion and tsunami simulation, Bull. Seismol. Soc. Am. 106, no. 4, 1652–1662.

Stafford, P. (2022). A model for the distribution of response spectral ordinates from New Zealand crustal earthquakes based upon adjustments to the Chiou and Youngs (2014) response spectral model, Technical Rept. 2022/15, GNS Science, doi: 10.21420/5098-0S19.

Strasser, F. O., M. Arango, and J. J. Bommer (2010). Scaling of the source dimensions of interface and intraslab subduction-zone earthquakes with moment magnitude, Seismol. Res. Lett. 81, no. 6, 941–950.

Thurber, C., and D. Eberhart-Phillips (1999). Local earthquake tomography with flexible gridding, *Comput. Geosci.* **25,** no. 7, 809–818.

Uieda, L., D. Tian, W. J. Leong, L. Toney, W. Schlitzer, M. Grund, D. Newton, M. Ziebarth, M. Jones, and P. Wessel (2021). Pygmt: A python interface for the generic mapping tools, available at https://www.pygmt.org/ (last accessed December 2023).

Van Houtte, C., S. Bannister, C. Holden, S. Bourguignon, and G. McVerry (2017). The New Zealand strong motion database, *Bull. New Zeal. Soc. Earthq. Eng.* **50,** no. 1, 1–20.

Weber, B., J. Becker, W. Hanka, A. Heinloo, M. Hoffmann, T. Kraft, D. Pahlke, J. Reinhardt, J. Saul, H. Thoms, *et al.* (2007). Seiscomp3-automatic and interactive real time data processing, *Geophys. Res. Abstr.*, Vol. 9, 219 pp.

Wessel, P., J. Luis, L. Uieda, R. Scharroo, F. Wobbe, W. H. Smith, and D. Tian (2019). The generic mapping tools version 6, *Geochem. Geophys. Geosys.* **20,** no. 11, 5556–5564.

Williams, C. A., D. Eberhart-Phillips, S. Bannister, D. H. Barker, S. Henrys, M. Reyners, and R. Sutherland (2013). Revised interface geometry for the hikurangi subduction zone, New Zealand, *Seismol. Res. Lett.* **84,** no. 6, 1066–1073.

Worden, C., M. Gerstenberger, D. Rhoades, and D. Wald (2012). Probabilistic relationships between ground-motion parameters and modified mercalli intensity in California, *Bull. Seismol. Soc. Am.* **102,** no. 1, 204–221.

Wotherspoon, L., A. Kaiser, E. Manea, and A. Stolte (2022). National seismic hazard model: Site characterisation database summary report, *Technical Rept. 2022/28*, GNS Science, doi: 10.21420/363X-CK83.